J. Fluid Mech. (1995), *vol.* 298, *pp.* 1–22

A vertically oscillating plate disturbing the development of a boundary layer

By J. J. MIAU[1], C. R. CHEN[1] AND J. H. CHOU[2]

[1] Institute of Aeronautics and Astronautics, National Cheng Kung University, Tainan, Taiwan, Republic of China

[2] Department of Engineering Science, National Cheng Kung University, Tainan, Taiwan, Republic of China

(Received 6 June 1994 and in revised form 30 January 1995)

A vertically oscillating plate in a boundary layer regulates the vorticity flux rate with respect to time and displaces the vorticity away from the wall. These phenomena are discussed for non-dimensional frequencies of the oscillating plate $K = 0$, 0.006, 0.01 and 0.02. The velocity data obtained by a split-fibre probe near the wall in the region immediately downstream of the oscillating plate lead to a discussion on the behaviour of the flow structures with respect to the non-dimensional frequency. The physical understanding deduced is complementary to the findings of a smoke-wire flow visualization conducted in this study. An integral analysis of the momentum equation indicates that the mean vorticity flux rate of the present flow is composed of contributions from both the parallel shear layer and the curving streamline. This analysis further suggests that the mean vorticity flux rate can be obtained through a combination of pressure measurements at the wall and in the irrotational region of the flow.

1. Introduction

This paper is concerned with the development of unsteady vortical structures downstream of a vertically oscillating plate which projects into a steady flow over a flat plate. The present configuration is relevant to considerations of a high lift device for aerodynamic flows and control of flow separation. With an oscillating plate installed on the upper surface of a NACA 0012 airfoil, Francis *et al.* (1979) found that the aerodynamic performance of the airfoil at zero angle of attack bears a resemblance to that of a pitching airfoil in a dynamical stall situation. Koga (1983), Nagib, Reisenthel & Koga (1985), and Reisenthel, Nagib & Koga (1985) illustrated that by installing an oscillating flap in the flow separation region, the reattachment length of the separated flow could be reduced significantly. Reynolds & Carr (1985) performed a review of various configurations of unsteady driven separated flows. Their interpretation of Francis *et al.*'s and Koga's findings is that either the oscillating plate or the oscillating flap generates vorticity as flow passes over the tip and produces a separated flow. The oscillating device provides an environment for the accumulation of vorticity, namely the forming of vortical structures. Miau & Chen (1991), Miau, Chen & Chou (1991*a*) and Miau *et al.* (1991*b*) performed a series of experiments on a boundary layer disturbed by an oscillating plate. Notable results of these studies can be briefly described as follows. Miau *et al.* (1991*a*) found a critical frequency of the oscillating plate that differentiates two flow regimes: below this frequency the separated shear layer behaves in a quasi-steady manner similar to the case with a fixed plate, and

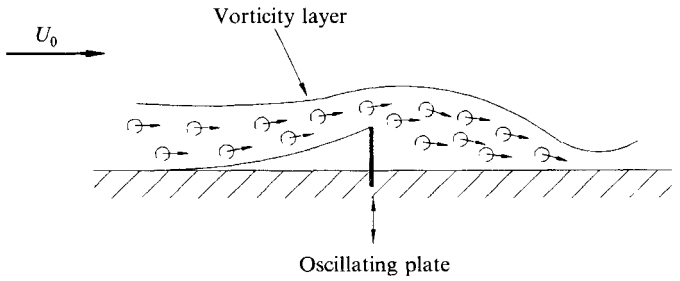

FIGURE 1. A schematic drawing of the vorticity layer disturbed by an oscillating plate.

above it the separated shear layer develops into a vortical structure. Miau *et al.* (1991*b*) placed an oscillating plate upstream of a backward-facing step to control the separated flow. They found that the reduction of the reattachment length could be more than 40%.

In this study, a boundary layer is viewed as a vorticity layer. A general description of the present flow can be given with the assistance of figure 1. Far upstream of the vertically oscillating plate, a thin vorticity layer, i.e. the boundary layer, is characterized by constant vorticity flux rate. As the flow approaches the oscillating plate, the vorticity flux rate decreases owing to the presence of an adverse pressure gradient. Then, closer to the oscillating plate, the vorticity layer detaches from the wall surface and curves around the oscillating plate. In the neighbourhood of the tip of the oscillating plate, i.e. in the presence of a favourable pressure gradient, vorticity is generated from the oscillating plate. Downstream of the oscillating plate the development of the vorticity layer, which is the main interest of the present work, is complicated and depends heavily on the non-dimensional frequency of the oscillating plate.

Based on the above description, the effects of the oscillating plate on the development of boundary layer flow can be summarized into two aspects. One is vorticity generation by the oscillating plate and the other is vorticity redistribution in the downstream flow due to the action of the oscillating plate. The latter effect can also be seen as the oscillating plate regulating the vorticity flux rate with respect to time in addition to displacing vorticity away from the wall. In this work, experiments were carried out to help in understanding the flow phenomena mentioned above.

2. Experimental method

2.1. *Facility*

A low-speed wind tunnel was employed for the present study. The test section is 150 mm by 150 mm in cross-section. Descriptions of this wind tunnel in detail can be found in Miau *et al.* (1991*a*).

A schematic sketch of the present flow configuration and the coordinate system employed are given in figure 2. The oscillating plate shown in the figure is in simple harmonic motion, with frequency up to 15 Hz. The maximum height of the oscillating plate, denoted H, was 10 mm for velocity and pressure measurements, and 13.5 mm for flow visualization experiments. The minimum height of the oscillating plate was zero, corresponding to the situation that the plate was completely retracted into the wall surface. The spanwise length of plate was 150 mm.

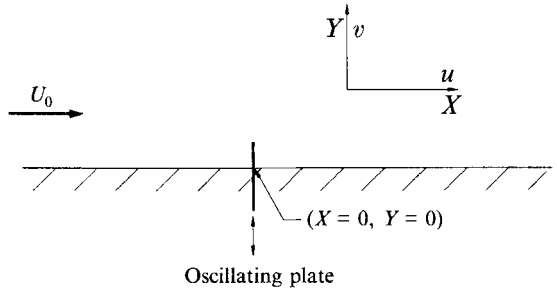

FIGURE 2. A schematic drawing of the flow configuration and the coordinate system employed.

2.2. *Experimental technique and data processing*

A smoke-wire flow visualization technique was employed for revealing the vortical structures produced by the oscillating plate. This technique is described in Miau *et al.* (1991*b*). In the present work, the flow visualization experiments were done at $U_0 = 1\ \mathrm{m\ s^{-1}}$, where U_0 denotes the free-stream velocity measured at the inlet of the test section. The highest non-dimensional frequency K achieved is 0.15. K is defined as fH/U_0 where f is the oscillating frequency of the plate.

An X-type hot-wire probe was employed to measure the instantaneous velocity components in the streamwise and vertical directions. Measurements were performed in the centreline plane of the test section. A phase-averaging procedure referred to the phase of the oscillating motion of the plate was adopted to reduce the ensemble-averaged velocity data at each of the positions measured. The reference phase $t/T = 0$, i.e. $\theta = 0°$ or 360°, denotes the instant when the plate is completely retracted into the wall and $t/T = \frac{1}{2}$, i.e. $\theta = 180°$, denotes the instant when the plate reaches its maximum height. T corresponds to the period of plate oscillation. Consequently, a collection of the ensemble-averaged velocity data obtained at the measurement points in the flow field, referred to a specified phase, is able to show the two-dimensional flow structure. It should be mentioned that the present work tends to view the unsteady flow structures produced as two-dimensional. Rigorously speaking, the latest measurements performed showed that the existence of the sidewalls causes the shedding vortices to become more three-dimensional downstream. For instance, at $K = 0.006$ and 0.02 the ensemble-averaged flow structures show two-dimensional behaviour within the spanwise regions $-3 < Z/H < 3$ and $-5 < Z/H < 5$, respectively, at the streamwise position $X/H = 25$. Hence, as the K value gets lower, the two-dimensional region of the flow structure in the spanwise direction gets narrower. The results reported in the present paper are limited to the streamwise region $X/H < 30$.

The ensemble-averaged velocity data were utilized to obtain the vorticity by reduction. This was achieved by differentiating the ensemble-averaged velocity profiles obtained at two streamwise locations 1 mm apart. The ensemble-averaged spanwise vorticity was calculated from the following expression:

$$\langle \omega_z \rangle = \frac{\partial \langle u \rangle}{\partial Y} - \frac{\partial \langle v \rangle}{\partial X}, \tag{1}$$

where $\langle u \rangle$ and $\langle v \rangle$ denote the ensemble-averaged velocity components in the X- and Y-directions, respectively.

The near-wall velocity was acquired by a split-fibre probe because of the presence of reversed flow near the wall (Kiya & Sasaki 1983). The flow direction was then deduced by comparing the velocities measured by the platinum-coated films: the velocity on the

windward side should be higher than the velocity on the leeward side. In this experiment, data obtained by the split-fibre probe were ensemble-averaged over 500 samples to reduce to the mean velocity. The reattachment point can be defined as the point where the probabilities of forward and backward flows are equal (Eaton & Johnston 1982). Here, the probability of forward flow F_p is defined as follows:

$$F_p = N_{forward}/N_{total},$$

where $N_{forward}$ is the number of samples of forward velocity, and N_{total} the total number of samples. Hence, $F_p = 0$ denotes a complete reversed flow situation and $F_p = 1$ a totally forward flow situation.

Wall pressure measurements were made in the regions upstream and downstream of the oscillating plate. Wall pressure taps, 1 mm in diameter, were arranged every 10 mm in the streamwise direction along the centreline of the test section wall. Pressure measurements were made by a diaphragm-type pressure transducer. The pressure coefficient C_p was calculated with reference to the pressure measured 250 mm upstream of the oscillating plate when the plate height is zero. Following the phase-averaging procedure described above, the ensemble-averaged pressure referred to the phase of the oscillating plate could be deduced. A condenser microphone was employed to correct the phase lag in the signals of the diaphragm pressure transducer, which was due to the characteristic response of the transducer.

In the present study the Reynolds number is defined based on U_0 and H. For the velocity and wall pressure measurements the Reynolds number was held at 3.1×10^3. Under this flow condition, i.e. $U_0 = 5\ \mathrm{m\ s^{-1}}$, the boundary layer thickness, displacement thickness, momentum thickness and shape factor measured at $X = 0$, in the absence of the oscillating plate, are 6.5 mm, 2.1 mm, 0.8 mm and 2.72 respectively. For the flow visualization experiments, the Reynolds number was held at 8.4×10^2 for $U_0 = 1\ \mathrm{m\ s^{-1}}$. For this case, the boundary layer thickness, displacement thickness, momentum thickness and shape factor measured at $X = 0$, in the absence of the oscillating plate, are 12.5 mm, 4.7 mm, 1.8 mm and 2.64 respectively. In both cases, the boundary layers measured show laminar characteristics. Their velocity profiles appear to be very close to the Blasius boundary layer profile and the maximum turbulence intensities measured in the boundary layers are less than 1% of U_0.

In the following, it is found that the flow visualization results and the velocity/pressure data which were obtained at different Reynolds numbers show similar flow characteristics. However, this does not necessarily mean that these two sets of results imply Reynolds number similarity in the range of Reynolds numbers between the two experimental conditions studied. The Reynolds number effect on the present flow phenomena is an area that needs to be investigated in the future.

3. Global features of the flow

3.1. *Flow visualization*

The general characteristics of the flow downstream of the oscillating plate can be described using the smoke-wire visualization photographs shown in figure 3. At $K = 0$, i.e. the case of a fixed plate, shown in figure 3(*a*), the separated shear layer originated from the tip of the plate appears to convect downstream with the flow. The separated shear layer rolls up into vortices before reattachment on the wall.

For $K = 0.0067$, figure 3(*b*) shows a picture taken at $t/T = 0.42$, i.e. an instant at which the plate is moving toward the upper dead end, which suggests that the

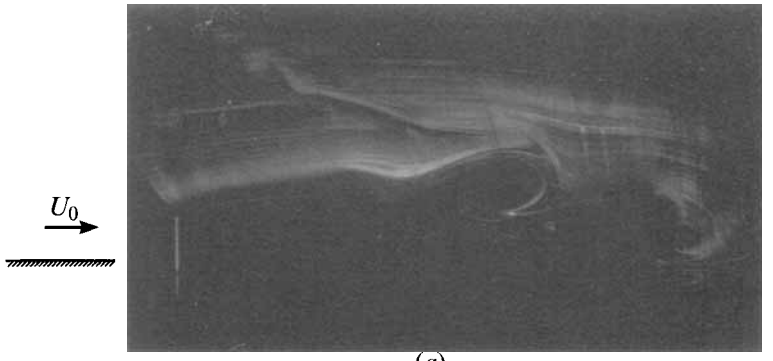

(*a*)

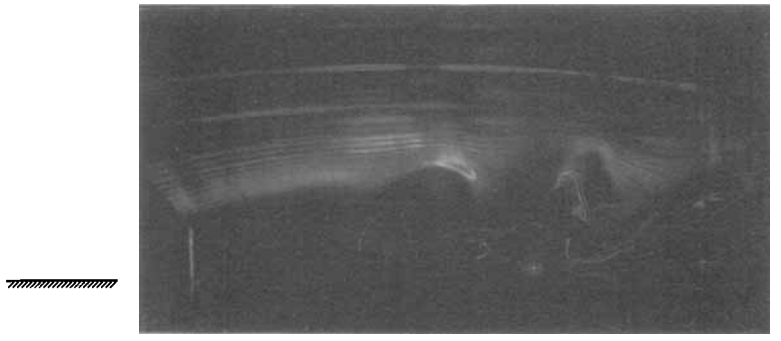

(*b*)

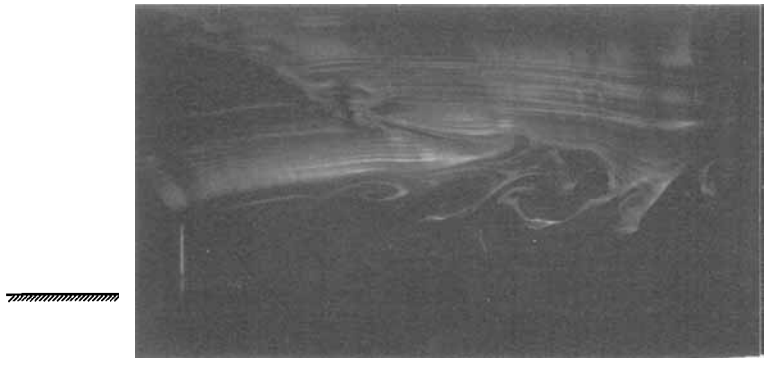

(*c*)

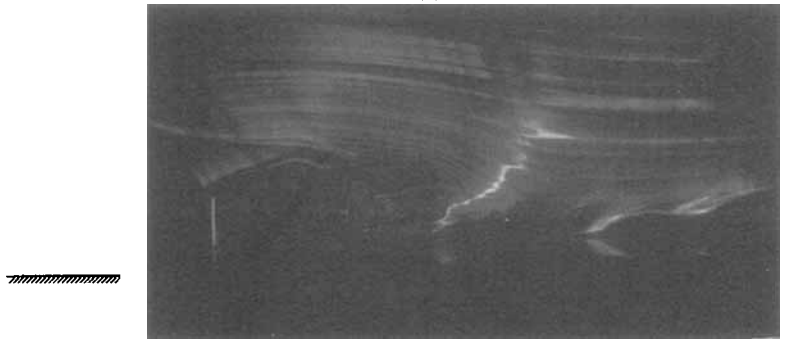

(*d*)

FIGURE 3(*a–d*). For caption see page 7.

(*e*)

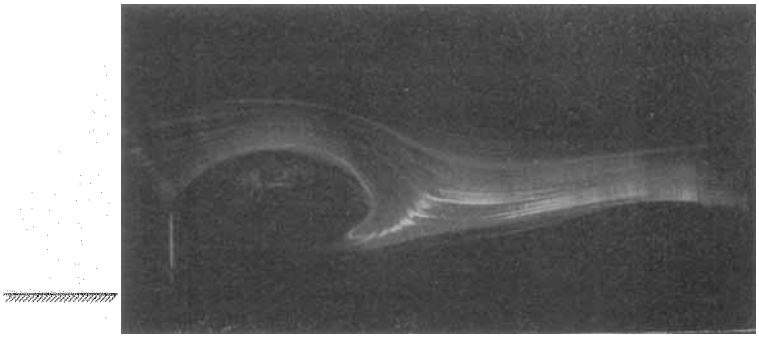

(*f*)

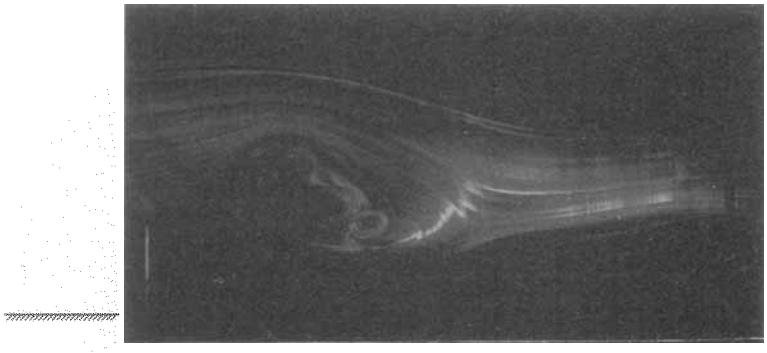

(*g*)

(*h*)

FIGURE 3(*e–h*). For caption see facing page.

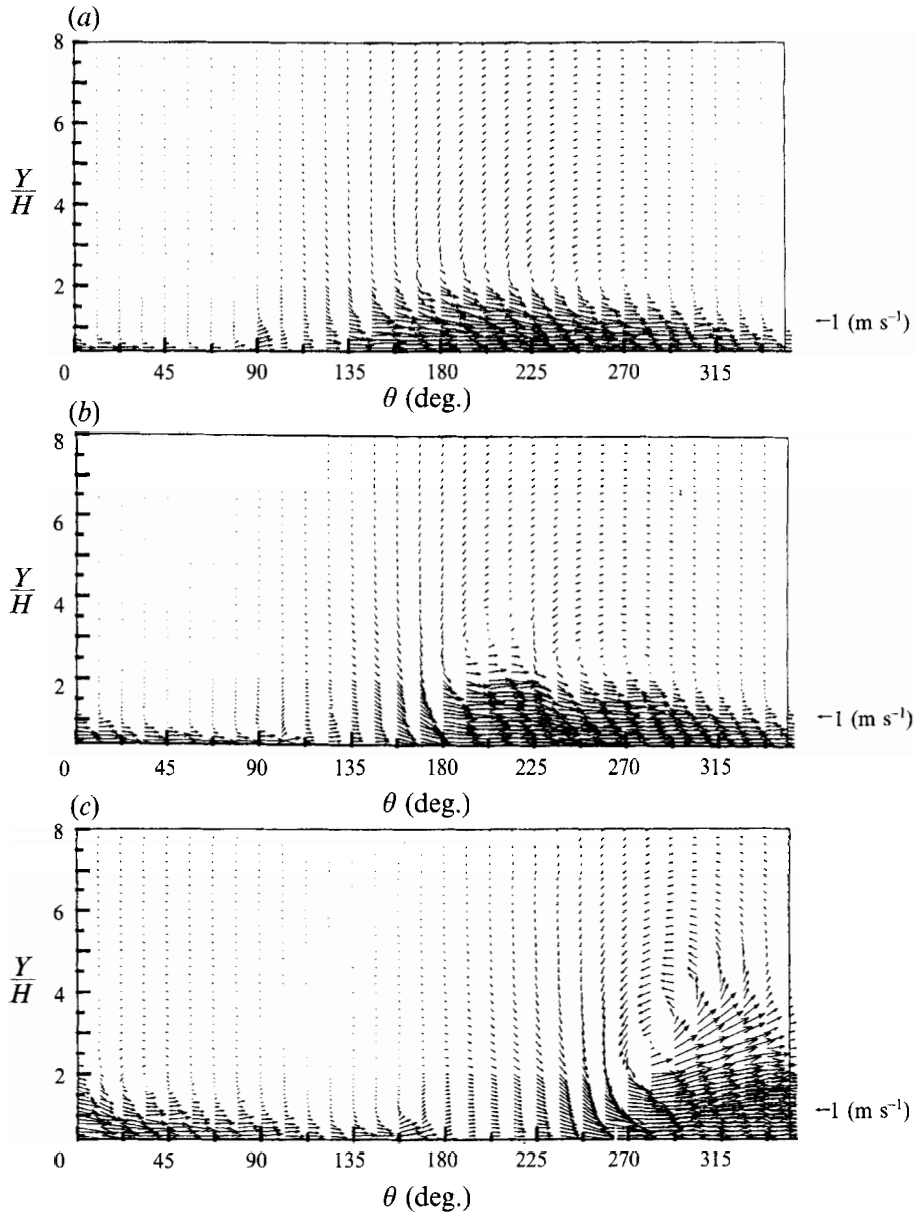

FIGURE 4. Ensemble-averaged velocity vector plots obtained at Reynolds number 3.1×10^3, at $X/H = 10$, for (*a*) $K = 0.006$; (*b*) $K = 0.01$ and (*c*) $K = 0.02$.

appearance of the separated shear layer is similar to that of the shear layer at $K = 0$. Figure 3(*c*) shows a picture taken at $t/T = 0.58$, i.e. an instant that the plate is retracting from the upper dead end, which indicates that the separated shear layer is being convected downstream in the form of shedding vortices.

FIGURE 3. Smoke-wire flow visualization photographs taken at Reynolds number 8.4×10^2, for (*a*) $K = 0$; (*b*) $K = 0.0067$, $t/T = 0.42$; (*c*) $K = 0.0067$, $t/T = 0.58$; (*d*) $K = 0.012$, $t/T = 0.44$; (*e*) $K = 0.012$, $t/T = 0.56$; (*f*) $K = 0.028$, $t/T = 0.5$; (*g*) $K = 0.028$, $t/T = 0.56$ and (*h*) $K = 0.14$, $t/T = 0.65$.

For $K = 0.012$, figure 3(*d*) presents a picture taken at $t/T = 0.44$. A comparison between figures 3(*d*) and 3(*b*) reveals that the increase of K from 0.0067 to 0.012 results in a shortening of the reattachment length associated with the separated shear layer. According to Miau *et al.* (1991*a*), $K = 0.009$ corresponds to a critical situation, above which vorticity in the shear layer accumulates in the process of the plate extending towards the upper dead end. The flow appearance of figure 3(*d*) basically confirms this statement that the separated shear layer tends to be held behind the oscillating plate, rather than convecting downstream. Figure 3(*e*) shows a photograph taken at $K = 0.012, t/T = 0.56$. At this instant the plate is in the retracting motion and the separated shear layer appears to convect downstream in the form of shedding vortices.

For $K = 0.028$, the photograph taken at $t/T = 0.5$ is given in figure 3(*f*), which clearly shows that the separated shear layer is held behind the oscillating plate in the form of a large-scale vortex. The photograph taken at a later instant $t/T = 0.56$, shown in figure 3(*g*), further reveals that as the plate retracts the separated shear layer shed from the tip of the plate is linked to the primary vortical structure which appears to be convecting downstream.

At even higher K, i.e. 0.14, a picture taken at $t/T = 0.65$ is shown in figure 3(*h*), indicating that a large-scale vortex is still held behind the oscillating plate although the plate is in the retracting motion, notably different from the appearance of the flow in figure 3(*g*).

In summary, flow visualization results presented in figure 3 show the effect of the non-dimensional frequency of the oscillating plate on the variations of the flow structures. At lower K, i.e. 0.0067, the flow behaves as in a quasi-steady situation. At $K = 0.012$, the separates shear layer is held behind the plate when the plate is in the extending motion, and sheds downstream in the form of multiple vortices when the plate is in retracting motion. At higher K, i.e. 0.028, the separated shear layer shed from the tip of the oscillating plate developed into a dominant large-scale vortex, which is detached from the plate shortly after it reaches the upper dead end. At the highest K shown in this figure, i.e. 0.14, the large-scale vortex does not shed from the plate until a later phase in the retracting motion.

The experimental observations described above can be futher explained in terms of vorticity accumulation. Since the shear layer originated from the plate tip contains vorticity, the growth of the vortex to accommodate the separated shear layer is considered as a process of vorticity accumulation. Vortex shedding takes place as the condition of saturation of vorticity accumulation is met, which depends on the state of the oscillating plate. As seen in figure 3(*h*), at $K = 0.14, t/T = 0.65$, the large-scale vortex does not shed even at the instant that the plate is in the retracting motion.

3.2. *Velocity field of the flow behind the oscillating plate*

Concerning the evolution of flow structures downstream of the oscillating plate, the trajectory of the flow structure is noted to deviate away from the wall more pronouncedly as K increases. This feature can be seen in figure 4 which presents the ensemble-averaged velocity vector plots for $K = 0.006$, 0.01, and 0.02 obtained at $X/H = 10$. In this figure, the free-stream flow convects from right to left and the velocity vectors plotted are equivalent to the ensemble-averaged velocities measured with $5\ \mathrm{m\ s^{-1}}$, i.e. U_0, subtracted. This plotting technique is useful to reveal the vortical structures in the flow.

For $K = 0.006$, the plot obtained at $X/H = 10$ shows that the disturbed flow produced by the oscillating plate is mainly confined in the region $Y/H < 3$. For $K = 0.01$, sizable vortical structures are identified in the plot obtained at $X/H = 10$,

with the vertical extent reaching $Y/H = 4$. For $K = 0.02$, the vortical flow structures seen at $X/H = 10$ appear to contain a much higher intensity of vorticity compared to $K = 0.006$ and 0.01. At $X/H = 10$ the vortical structure extends roughly to $Y/H = 5$. Among the three values of K shown in the figure, the vortical structure seen for $K = 0.02$ appears to move away from the wall most pronouncedly.

At $K = 0.01$, the vortical structure seen in figure 4(*b*) has the appearance of multiple cells, e.g. at $X/H = 10$ a cell is detected in the neighbourhood of the phase $\theta \approx 200°$ and another cell is centred at $\theta = 270°$. This agrees well with the appearance of the flow visualization photograph shown in figure 3(*e*), taken at $K = 0.012$, i.e. that multiple vortices are shed downstream as the plate is in the retracting motion.

4. Measurement of vorticity flux rate

The vorticity flux rate is found to be useful for describing the dynamic aspects of the present flow. The ensemble-averaged vorticity flux rate is shown in the expression

$$\langle \dot{I} \rangle = \int_0^\infty \langle \omega_z \rangle \langle u \rangle \, \mathrm{d}Y. \tag{2}$$

This expression was modified slightly in the present study to avoid a difficulty in using the X-type hot-wire probe, arising because the hot-wire probe could not get closer than 3 mm to the wall owing to its physical size. Therefore, the vorticity flux rate in this thin layer, $0 < Y < 3$ mm, is approximated by $\frac{1}{2}\langle u_a \rangle^2$, where $\langle u_a \rangle$ denotes the ensemble-averaged velocity at $Y_a = 3$ mm. This approximation is valid under the assumption of parallel flow near the wall. Hence,

$$\langle \dot{I} \rangle = \int_{Y_a}^\infty \langle \omega_z \rangle \langle u \rangle \, \mathrm{d}Y + \tfrac{1}{2}\langle u_a \rangle^2. \tag{3}$$

This quantity was evaluated at $X/H = 0$, 10, 20 and 30. It should be mentioned that the vorticity data at $X/H = 0$ were reduced from the velocity profiles obtained at the two streamwise locations $X = 1.5$ and 2.5 mm.

Figure 5 shows the ensemble-averaged patterns of the vorticity flux rate at $K = 0.006$, 0.01 and 0.02. In this figure, the quantity $\langle \dot{I} \rangle$ is normalized by $\frac{1}{2}U_0^2$ which is the vorticity flux rate of the boundary layer without the presence of the oscillating plate. Notable features found in this figure are described below.

First, for all the values of K studied, the ensemble-averaged vorticity flux rates obtained at $X/H = 0$ show a substantial increase between phases $\theta = 45°$ and 180°. This feature gets more pronounced as K increases. Since the phases from $\theta = 45°$ to 180° correspond to the instants when the plate is extending toward the upper dead position, the vorticity flux rates shown are associated with a thin shear layer shed from the tip of the oscillating plate. Chen (1991) showed that during this period of time, the velocity profile of the shear layer above the tip of the plate is characterized by an overshoot at the edge. Vorticity is confined in the shear layer, whereas flow above the overshoot position is found to be basically irrotational.

Second, the patterns of the ensemble-averaged vorticity flux rate shown in figure 5 appear to fluctuate at larger magnitude at higher K. For $K = 0.01$ and 0.02, large variations of vorticity flux rate are associated with the instants when the vortical structure passes through the measurement location, as seen from the velocity vector plots shown in figure 4. As noted, the vorticity flux rate decreases to a small value as

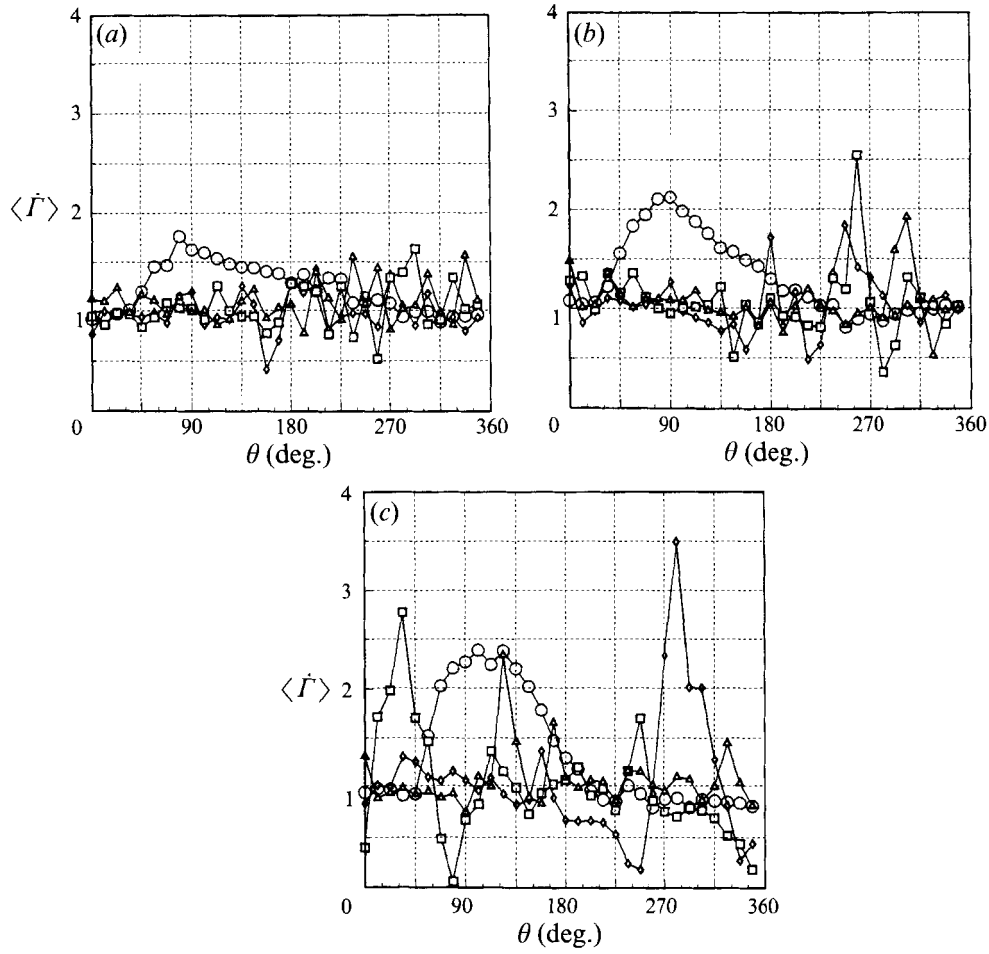

FIGURE 5. Ensemble-averaged vorticity flux rates obtained at Reynolds number 3.1×10^3, at various X/H for (*a*) $K = 0.006$; (*b*) $K = 0.01$ and (*c*) $K = 0.02$: ○, $X/H = 0$; ◇, $X/H = 10$; □, $X/H = 20$; △, $X/H = 30$.

the leading edge or the rear edge of the vortex passes through the measurement location, whereas the vorticity flux rate reaches a maximum value as the core of the vortex passes.

To further explore the flow characteristics of the vortical structure, a set of ensemble-averaged velocity and vorticity profiles obtained at $X/H = 20$, for $K = 0.02$, at the phases $\theta = 348°$ and 33° are shown in figure 6. Referring to figure 5(*c*), one sees that at the phases $\theta = 348°$ and 33° the minimum and maximum vorticity flux rates are found, respectively. At $\theta = 348°$, the ensemble-averaged streamwise velocity profile shown in figure 6(*a*) reveals that the streamwise velocity profile appears to be rather flat, and a moderate velocity gradient occurs over a vertical extent of roughly $Y/H < 5$. At $\theta = 33°$, the ensemble-averaged streamwise velocity profile shown in figure 6(*b*) indicates that a strong velocity gradient exists within $Y/H = 4$ to 6, which reflects the characteristic of the core of the vortical structure. From figure 6 it is also found that the velocities of the vertical components measured in the vortical structure are not negligible. This implies that the assumption of parallel flow does not apply to the region of vortical flow.

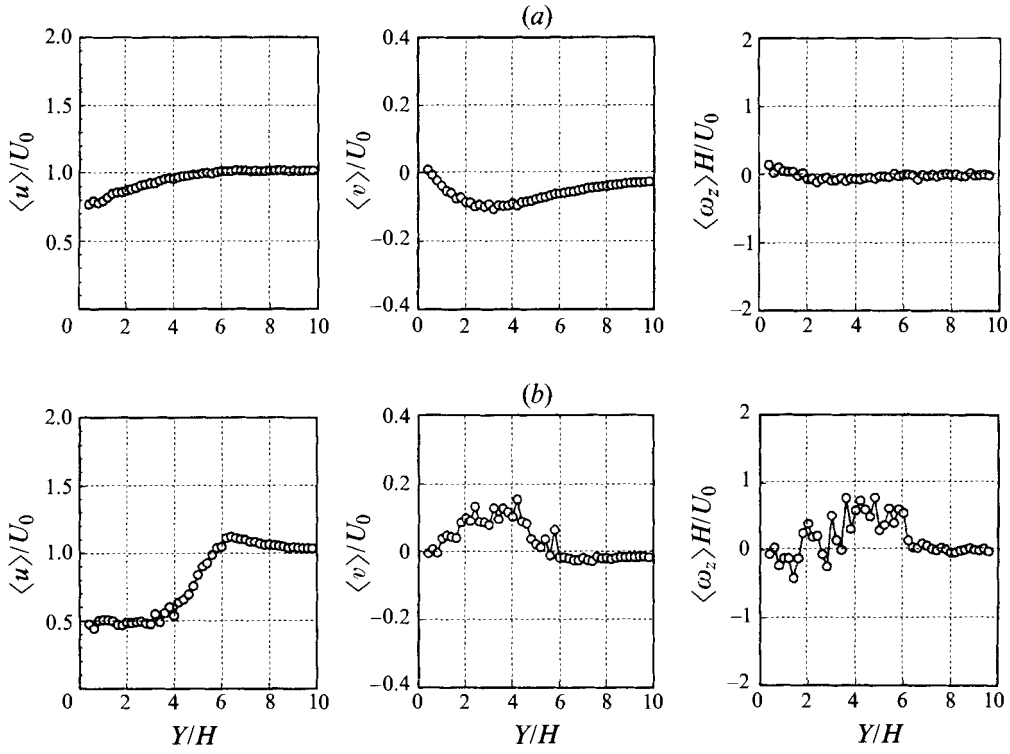

FIGURE 6. Ensemble-averaged velocity profiles and vorticity profiles at $X/H = 20$, for $K = 0.02$ and Reynolds number 3.1×10^3, at phases (*a*) $\theta = 348°$, (*b*) $\theta = 33°$.

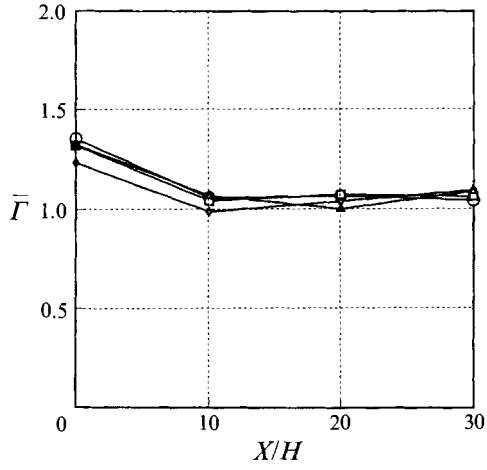

FIGURE 7. The distribution of the time-mean vorticity flux rates at $X/H = 0$, 10, 20 and 30 for various K: ○, $K = 0$; ◇, $K = 0.006$; □, $K = 0.01$; △, $K = 0.2$.

By integrating the ensemble-averaged vorticity flux rate shown in figure 5 over the period T, namely $\theta = 0°$ to 360°, the resultant value is equivalent to the total vorticity flux rate over a cycle of plate oscillation. This quantity is further normalized in the following form:

$$\bar{\Gamma} = \int_0^T \langle \dot{\Gamma} \rangle \, \mathrm{d}t / (\tfrac{1}{2} U_0^2 \, T). \tag{4}$$

$\bar{\Gamma}$ is also a time-mean quantity of the vorticity flux rate.

The values of $\bar{\Gamma}$ obtained for $K = 0.006$, 0.01 and 0.02 at $X/H = 0$, 10, 20 and 30 are plotted in figure 7. The three values of K studied show the general feature that while the values of $\bar{\Gamma}$ obtained at $X/H = 0$ are greater than 1, those obtained at $X/H = 10$, 20 and 30 appear to be comparable to 1. This trend implies that vorticity generation due to the oscillating plate appears to affect the local flow; further downstream the vorticity flux rate tends to return to that of the flat-plate boundary layer. Plausibly, this behaviour is due to the production of vorticity of opposite sign at the solid boundary in the region of recirculating flow and in the neighbourhood of the reattachment of the separated flow structure where the adverse pressure gradient exists.

5. Vorticity distribution downstream of the oscillating plate

In view of one of the effects of the oscillating plate being to displace the vorticity of the flow away from the wall, a definition of vorticity distribution factor, $\langle D_\omega^* \rangle$, is proposed for describing this effect in a quantitative manner:

$$\langle D_\omega^* \rangle = \int_0^\infty \langle \omega_z \rangle \, Y \, \mathrm{d}Y/(U_0 H). \tag{5}$$

Equation (5) indicates that $\langle D_\omega^* \rangle$ is a quantity involving the Y-moment of the ensemble-averaged vorticity. Since vorticity in the present flow is considered to play the role of inducing free-stream fluid to move toward the wall, this quantity in some sense describes the effectiveness of vorticity in momentum transport. The ensemble-averaged patterns of $\langle D_\omega^* \rangle$ obtained at $X/H = 0$, 10, 20 and 30 for $K = 0.006$, 0.01 and 0.02 are shown in figure 8. The similar appearance of figures 8 and 5 is attributed to the large-scale variations seen in the plots of both figures being associated with the convection of flow structures produced by the oscillating plate. On the other hand, a discrepancy between figures 8 and 5 is also noted. In figure 5(*c*), for $K = 0.02$, the maximum vorticity flux rate found at $X/H = 10$ is seen to be greater than that at $X/H = 20$, whereas in figure 8(*c*), for the same K, the maximum vorticity distribution factor found at $X/H = 10$ is less than that at $X/H = 20$. This discrepancy is attributed to the vortical structure moving rapidly away from the wall for $K = 0.02$. Further downstream, at $X/H = 30$, both the maximum vorticity flux rate and the maximum vorticity distribution factor are smaller than those at $X/H = 20$. Based on the above comparison, it is suggested that the strength of the vortical structure is decaying from $X/H = 20$ to 30.

Figure 8(*d*) compares the time-mean values of $\langle D_\omega^* \rangle$, denoted $\bar{D}_\omega^*$, at $X/H = 0$, 10, 20 and 30 for the three values of K studied. The time-mean values are noted to be much greater than the reference level plotted, which corresponds to the flat-plate boundary layer flow in the absence of the oscillating plate. Generally speaking, the higher the K value the greater the $\bar{D}_\omega^*$ value is. For $K = 0.006$ and 0.01, the maximum $\bar{D}_\omega^*$ value is found at $X/H = 0$, but for $K = 0.02$ the maximum value is at $X/H = 10$. This difference is attributed to the fact that at $K = 0.02$ the vortex produced by the oscillating plate is much more organized and moves farther away from the wall. A comparison of figures 7 and 8(*d*) clearly shows that the vorticity displacement due to the oscillating plate is pronounced despite the time-mean vorticity convection rate being maintained at the same level as for the flat-plate boundary layer in the region $X/H = 10$ to 30. Figure 8(*d*) also shows that the $\bar{D}_\omega^*$ value level off at $X/H = 20$ and 30 for the three K values studied. This trend is in good agreement with the observation on the $\langle D_\omega^* \rangle$ results in the previous paragraph.

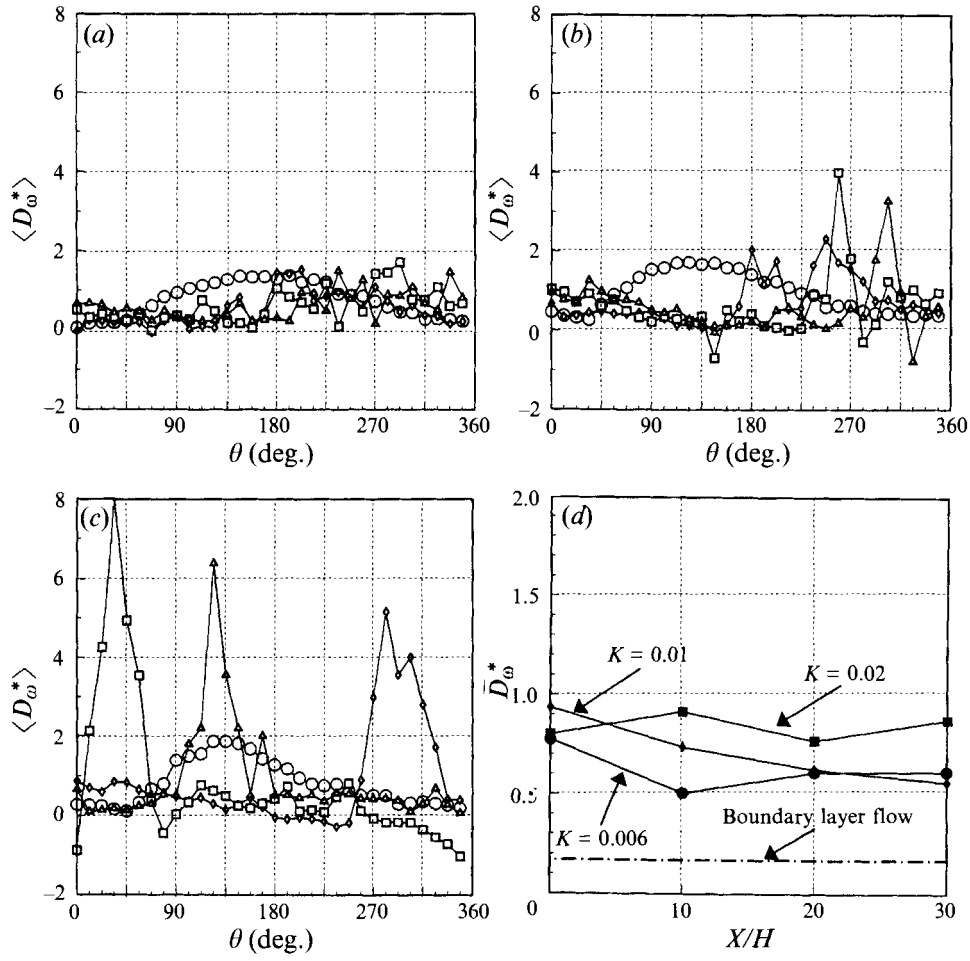

FIGURE 8. The variations of the ensemble-averaged vorticity distribution factor at various X/H for (*a*) $K = 0.006$; (*b*) $K = 0.01$, (*c*) $K = 0.02$ and (*d*) the distributions of $\bar{D}_\omega^*$ versus X/H: ○, $X/H = 0$; ◇, $X/H = 10$; □, $X/H = 20$; △, $X/H = 30$.

6. Flow development in the region immediately downstream of the oscillating plate

The flow visualization pictures shown in figure 3 reveal that the development of flow structure in the region immediately downstream of the oscillating plate is complicated. In this section, further velocity measurements in this region using a split-fibre probe and wall pressure distributions obtained along the wall are reported which reveal that the near-wall flow characteristics are well correlated with the flow structures produced by the oscillating plate.

6.1. *Near-wall velocity measurement*

Near-wall velocity data were obtained by a split-fibre probe traversing 1 mm above the wall surface. Of particular interest in the split-fibre data are the streamwise locations at which the velocity is zero and the probabilities of forward flow measured are 50%. In the following the measurement results for $K = 0.006$, 0.012, 0.016 and 0.02 are presented. Further discussion on the data will be given in §6.2. The split-fibre measurements were made every $0.5H$ in the streamwise direction.

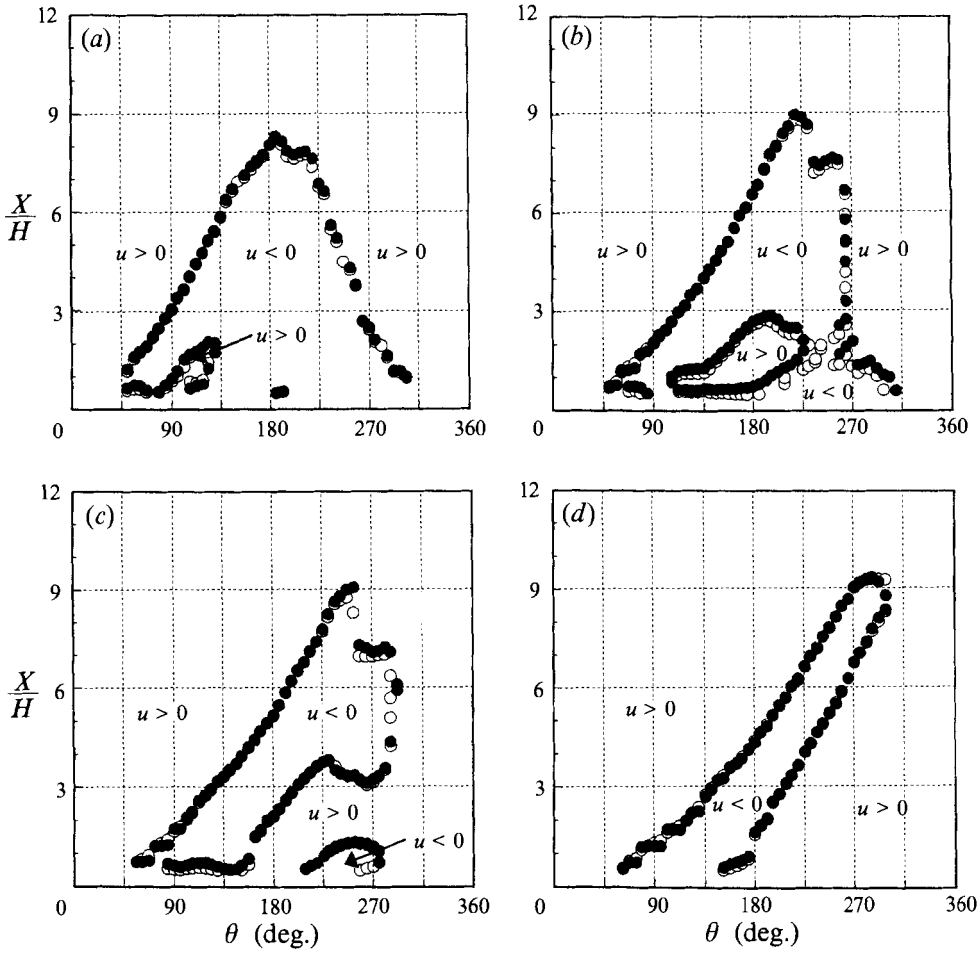

FIGURE 9. The streamwise locations corresponding to the zero ensemble-averaged velocity and the 50% forward flow probability measured versus θ, for (*a*) $K = 0.006$; (*b*) $K = 0.012$; (*c*) $K = 0.016$ and (*d*) $K = 0.02$: ○, $\langle u \rangle = 0$; ●, $F_p = 50\%$.

For the case of a fixed plate, the separated region is characterized by low-speed reversed flow. The reattachment lengths taken from the mean velocity data and the distribution of forward flow probability almost coincide: about $X = 6.7H$. For $K = 0.006$, shown in figure 9(*a*), the solid circles denote the streamwise locations at which the forward flow probabilites measured are 50% and the open circles denote the streamwise locations where the ensemble-averaged velocities measured are zero. It is seen that the results obtained by these two methods are in good agreement, supporting the statement made by Eaton & Johnston (1982). At the phases from $\theta = 45°$ to 135°, multiple zero-velocity points are identified along the wall. The outermost zero-velocity points shown in the figure, i.e. the distribution of the reattachment points, appear nearly symmetric with respect to $\theta = 180°$. This confirms the statement made by Miau *et al.* (1991*a*) that in this case the flow behaves in a quasi-steady manner. The maximum reattachment length shown in the figure is $8.2H$, which is longer than that for $K = 0$.

For $K = 0.012$, the maximum reattachment length taken from figure 9(*b*), which occurs at $\theta = 220°$, is about $9H$. This length is greater than that for $K = 0.006$. In this

FIGURE 10. Sketches depicting the situations at (*a*) the impingement (reattachment) point, (*b*) the separation point.

figure a drastic retracting of the reattachment points takes place at $\theta = 232°$, after the maximum reattachment length is reached. Also, note that the distribution of the reattachment lengths appears non-symmetric with respect to $\theta = 220°$. The ascending slope of the distribution of the reattachment length at phases from $\theta = 45°$ to 225° appears to be much more gradual than the descending slope of the reattachment length at $\theta = 225°$ to 260°.

For $K = 0.016$, figure 9(*c*) reveals that a drastic shortening of the reattachment length takes place at $\theta = 260°$, which is slightly delayed in phase compared to the case $K = 0.012$ already mentioned. The third zero-velocity point is measured at phases $\theta > 200°$, i.e. the oscillating plate is in the downstroke motion. This is somewhat different from what is seen at $K = 0.006$ and 0.012, where the third zero-velocity point is sensed at $\theta < 180°$, i.e. the oscillating plate is in the upstroke motion. In figure 9(*c*) at $\theta = 160°$ to 225°, the streamwise distance between the first and second zero-velocity points measured appears to remain constant. For $\theta > 225°$, this distance increases. For $\theta > 293°$, no zero-velocity point or reversed flow is identified near the wall.

For $K = 0.02$, figure 9(*d*) shows that two zero-velocity points are sensed near the wall at phases from $\theta = 152°$ to 293°. The streamwise distance between the first and second zero-velocity points measured remains almost constant through out these phases. The maximum reattachment length read from this figure is $9.2H$, which occurs at about $\theta = 300°$.

6.2. *Correlation between zero-velocity points and vortex development*

Studying the behaviour of the zero-velocity points near the wall is useful to trace the motion of vortical structures (Kiya & Sasaki 1985). The physical correspondence between the zero-velocity points and flow structures behind the oscillating plate is discussed in this section. Referring to figure 9(*a–d*), the outermost zero-velocity points shown in the plots should correspond to a situation of flow impingement (reattachment), indicated by the sketch in figure 10(*a*), while the next inner zero-velocity points measured (the second zero-velocity points) should correspond to a situation of flow separation, indicated by the sketch in figure 10(*b*). Similarly, the third zero-velocity points should correspond to a situation of flow impingement.

The outermost reattachment point can be regarded as the signature of the leading edge of the primary vortex. The higher the K value the more organized the vortical structure formed downstream of oscillating plate, so the reversed-flow region induced by the primary vortex is sustained even at phases $\theta > 180°$. The drastic shortening of the reattachment length after the maximum reattachment length is reached results from the primary vortex shedding from the flow separation region; hence this behaviour appears to be more significant at higher K.

The presence of the second zero-velocity point (separation point) can be explained as induced by the primary vortex, which the highly rotating fluid causes to lift from the wall surface, depicted by the sketch in figure 11. This phenomenon was also described by Doligalski & Walker (1984). Therefore, the length scale of the primary vortex is tentatively related to the streamwise distance between the reattachment point and the separation point. A comparison of figures 9(*b*) to 9(*d*) show that as K increases, the

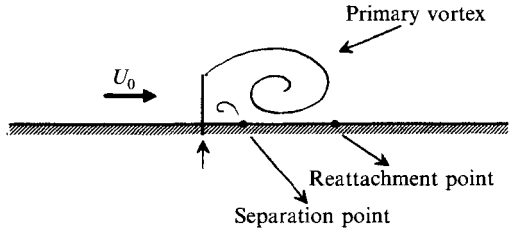

FIGURE 11. A sketch depicting the reattachment point and the separation point induced by the primary vortex.

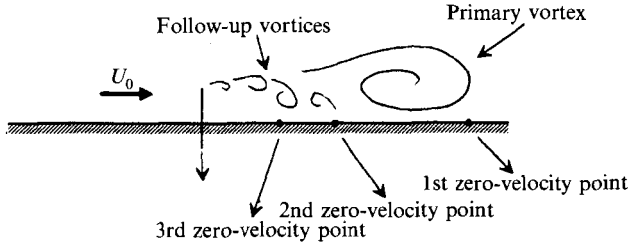

FIGURE 12. A sketch depicting the third zero-velocity point induced by the follow-up vortices.

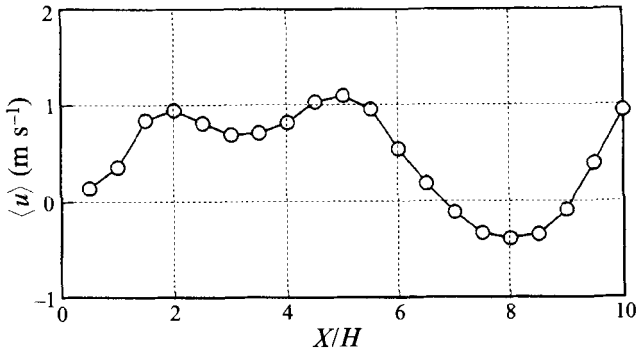

FIGURE 13. Ensemble-averaged near-wall velocity distribution obtained at $\theta = 270°$ for $K = 0.02$.

streamwise distance between the reattachment point and the separation point decreases. This can also be seen from figure 3 which shows that at lower K the primary vortex is not well organized but existed in a broader region. At higher K the primary vortex appears to be well organized. The scale of the primary vortex decreases as K increases. Further qualitative comparison regarding the scales of vortical structures versus K could be possible if the velocity measurements away from the wall in this region were obtainable.

The existence of a third zero-velocity point near the wall is noted for $K = 0.016$ or lower. The sketch given in figure 12 explains this phenomenon further. Figure 12 depicts the third zero-velocity point as being induced by the shedding of vortical structures following the primary vortex. While the phenomenon of multiple shedding of vortices in the shear layer is seen at $K = 0.0067$ to 0.028 in figure 3, higher the K value the more organized the primary vortex appears but the weaker the strength of the follow-up vortices in the shear layer. In figure 13 the streamwise distribution of the near-wall velocities measured at $K = 0.02$ shows that two zero-velocity points at $X/H = 6.8$ and 9.1 are identified to be the separation and reattachment points

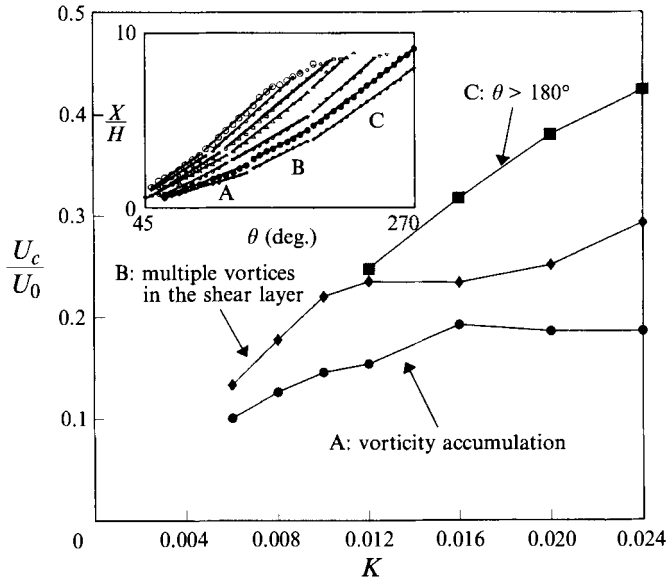

FIGURE 14. Variations of the convection speeds of the reattachment points with respect to K and θ. K values of the curves in the inset are, from top to bottom: 0.006, 0.008, 0.01, 0.012, 0.016, 0.02 and 0.024.

associated with the primary vortex structure. Further noted is a local minimum at $X/H = 3$, which is suggested to be due to the follow-up shedding vortices. However, the strength of these vortices is apparently not strong enough to induce a reversed flow near the wall. For this reason, the existence of the third zero-velocity point is found at $K = 0.016$ or lower.

For all the K values studied in the present work, the convection speeds of the reattachment points, which can be estimated from the data shown in figure 9, are not constant with respect to θ. The variations of the convection speeds of the reattachment points with respect to K for θ in the different ranges are described in figure 14. When θ is small, the convection speed is found to be low, which is mainly due to the vorticity accumulation in the primary vortex. This flow behaviour was also observed by Koga (1983). Later, but while the oscillating plate is still in the upstroke motion, the speed increases which corresponds to a stage where the separated shear layer appears to contain multiple vortices. When the plate is in the downstroke motion ($\theta > 180°$), the convection speed appears to be even faster.

6.3. *Variations of wall pressure distribution*

Wall pressure distributions obtained for $K = 0$, 0.006, 0.01 and 0.02 are presented in figure 15. In this figure, the ensemble-averaged pressure coefficient, $\langle C_p \rangle$, is defined as

$$\langle C_p \rangle = (\langle p \rangle - p_0)/(\tfrac{1}{2}\rho U_0^2) \tag{6}$$

where p_0 denotes the reference pressure measured upstream of the oscillating plate when the plate height is zero, $\langle p \rangle$ denotes the ensemble-averaged pressure measured, and ρ is the density of air.

In the fixed-plate case, figure 15(a) reveals that the C_p value measured in the recirculation zone is negative whereas the C_p value measured upstream of the plate is higher than 0. In comparison with the results obtained by the split-fibre probe it is

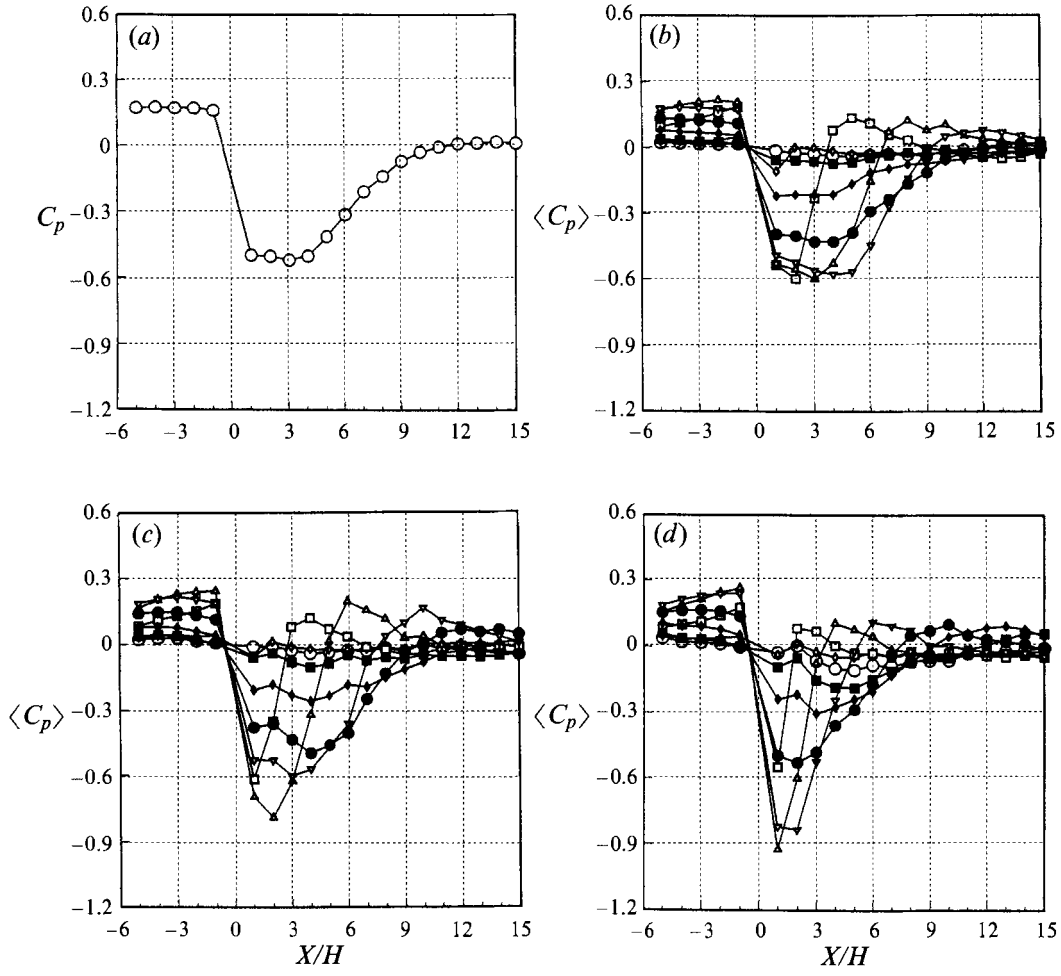

FIGURE 15. Ensemble-averaged wall pressure distributions obtained at Reynolds number 3.1×10^3, for (*a*) $K = 0$; (*b*) $K = 0.006$; (*c*) $K = 0.01$ and (*d*) $K = 0.02$: ○, $\theta = 0°$; ◇, $\theta = 45°$; □, $\theta = 90°$; △, $\theta = 135°$; ▽, $\theta = 180°$; ●, $\theta = 225°$; ◆, $\theta = 270°$; ■, $\theta = 315°$.

further found that the time-mean reattachment point $X/H = 6.7$ actually corresponds to a streamwise location at which the C_p value measured is lower than zero. In the neighbourhood of the reattachment point the slope of the C_p distribution is the largest, locally speaking.

A comparison of figures 15(*b*), 15(*c*) and 15(*d*) for $K = 0.006$, 0.01 and 0.02, respectively, shows the trend of the pressure distributions with respect to K. The higher the K value, the lower the minimum wall pressure. Also noted is that the streamwise location of the minimum wall pressure moves upstream with higher K, which implies that the vortical structure developed behind the oscillating plate reduces its size as K increases. Also noted for $K = 0.01$ and 0.02 is that the minimum wall pressure is found at $\theta = 135°$, at which the maximum suction effect occurs in the process of the vortex developing immediately behind the oscillating plate. At higher K the suction effect is more significant in the region near the oscillating plate, but its effective region get narrower.

6.4. *Correlation between wall pressure and vorticity flux rate*

The instantaneous vorticity flux rate of the present flow can be expressed in the following form:

$$\dot{\Gamma} = \int_0^h \omega_z u \, \mathrm{d}Y = \tfrac{1}{2}u_h^2 - \int_0^h u \frac{\partial v}{\partial X} \mathrm{d}Y, \tag{7}$$

where h denotes a vertical position far enough away from the wall so that the flow is irrotational; it is taken as $h = 7.5H$ in this study. The integrand in the second term of (7) is one of the convection terms in the v-component momentum equation. Therefore this term is further expanded using the expression for the momentum equation:

$$\dot{\Gamma} = \int_0^h u\omega_z \, \mathrm{d}Y = \tfrac{1}{2}u_h^2 - \int_0^h u \frac{\partial v}{\partial X} \mathrm{d}Y, \tag{8}$$

$$\int_0^h u \frac{\partial v}{\partial X} \mathrm{d}Y = -\int_0^h \frac{\partial v}{\partial t} \mathrm{d}Y - \int_0^h v \frac{\partial v}{\partial Y} \mathrm{d}Y - \int_0^h \frac{1}{\rho} \frac{\partial p}{\partial Y} \mathrm{d}Y - \int_0^h \nu \left(\frac{\partial^2 v}{\partial X^2} + \frac{\partial^2 v}{\partial Y^2} \right) \mathrm{d}Y$$

$$= -\int_0^h \frac{\partial v}{\partial t} \mathrm{d}Y - \frac{v_h^2}{2} - \frac{1}{\rho}(p_h - p_w) + \int_0^h \nu \frac{\partial^2 v}{\partial X^2} \mathrm{d}Y + \nu \frac{\partial v}{\partial Y}\bigg|_h, \tag{9}$$

$$\dot{\Gamma} = \underset{(a)}{\tfrac{1}{2}U_h^2} \underset{(b)}{- \frac{1}{\rho}(p_w - p_h)} + \underset{(c)}{\int_0^h \frac{\partial v}{\partial t} \mathrm{d}Y} \underset{(d)}{- \int_0^h \nu \frac{\partial^2 v}{\partial X^2} \mathrm{d}Y} \underset{(e)}{- \nu \frac{\partial v}{\partial Y}\bigg|_h}. \tag{10}$$

Note that p_w and p_h are pressures measured at the wall and $Y = h$, respectively; and ν is the kinematic viscosity. The terms (d) and (e) in (10) are of order $1/Re$ of the term (a) and are therefore neglected. Thus

$$\dot{\Gamma} = \tfrac{1}{2}U_h^2 - \frac{1}{\rho}(p_w - p_h) + \int_0^h \frac{\partial v}{\partial t} \mathrm{d}Y. \tag{11}$$

Equation (11) shows that the instantaneous vorticity convection rate comprises three terms: (i) $\frac{1}{2}U_h^2$ which is equivalent to the vorticity convection rate in a parallel shear flow (Sears 1956), (ii) $(1/\rho)(p_w - p_h)$ which is due to the streamline curving effect and (iii) $\int_0^h (\partial v/\partial t) \, \mathrm{d}Y$ which is due to the unsteady effect.

For a fixed plate, the normalized mean vorticity convection rate is

$$\bar{\Gamma} = \lim_{T \to \infty} \int_0^T \dot{\Gamma} \mathrm{d}t / (\tfrac{1}{2}U_\infty^2 T) = \left(\frac{\bar{U}_h}{U_\infty} \right)^2 + \frac{\overline{U_h'^2}}{U_\infty^2} - \frac{\bar{p}_w - \bar{p}_h}{\frac{1}{2}\rho U_\infty^2} \quad (\text{i.e. } U_h = \bar{U}_h + U_h')$$

$$= (\bar{U}_h/U_\infty)^2 - \bar{C}_{p_{wh}} \quad (\text{i.e. } \overline{U_h'^2}/U_\infty^2 \approx 0). \tag{12}$$

The unsteady term in (11) is eliminated because the plate is fixed.

For an oscillating plate, the normalized mean vorticity convection rate for one oscillating period is

$$\bar{\Gamma} = \int_0^T \dot{\Gamma} \mathrm{d}t / (\tfrac{1}{2}U_\infty^2 T)$$

(T is oscillating period) where

$$\dot{\Gamma} = \langle \dot{\Gamma} \rangle + \dot{\Gamma}'$$

$$= \left(\frac{\langle \bar{U}_h \rangle}{U_\infty} \right)^2 + \frac{\overline{U_h'^2}}{U_\infty^2} - \frac{\langle \bar{p}_w \rangle - \langle \bar{p}_h \rangle}{\frac{1}{2}\rho U_\infty^2} \quad (\text{i.e. } U_h = \langle U_h \rangle + U_h')$$

$$= (\langle \bar{U}_h \rangle / U_\infty)^2 - \langle \bar{C}_p \rangle_{wh}. \tag{13}$$

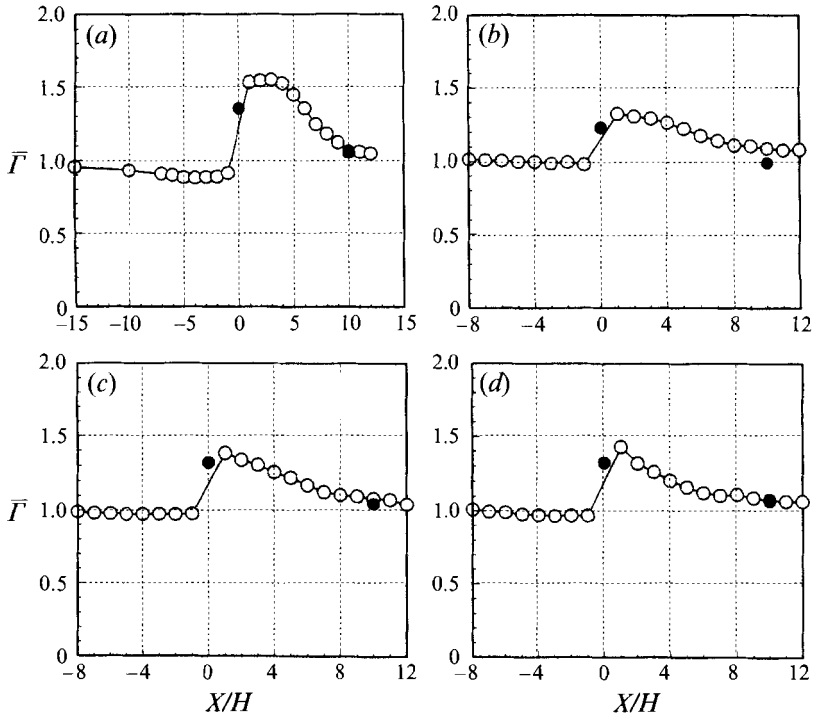

FIGURE 16. Comparison of the time-mean vorticity flux rates obtained by experiment and the integral analysis (13) for (*a*) $K = 0$; (*b*) $K = 0.006$; (*c*) $K = 0.01$ and (*d*) $K = 0.02$: ○, integral analysis; ●, experiment.

Similarly to (12), (13) shows that the mean vorticity convection rate for the case of the oscillating plate comprises two terms which are associated with the effect due to the parallel shear flow and the curving streamline. The two terms on the right-hand side of (13) can be estimated according to the data obtained from a Pitot tube traversing at $Y = h$ and the data on wall pressure measurements. Therefore, a comparison between the time-mean vorticity flux rate obtained from (13) and the previous result shown in figure 7 can be made, which is given in figure 16; the results match closely.

For a fixed plate, the normalized time-mean vorticity flux rate in the region upstream of the fixed plate ($X/H < -1$) is lower than 1 which is a reference level, plausibly due to the presence of an adverse pressure gradient. For the oscillating plate, figures 16(*b*) to 16(*d*) reveal that the normalized time-mean vorticity flux rate in region $X/H < 0$ is much closer to 1 than for the fixed plate. The reason for this is that the blockage effect due to the presence of the oscillating plate is weaker than for the fixed plate.

The increase of time-mean vorticity flux rate in the region $X/H = -1$ to 1 is caused by the vorticity generation and velocity acceleration in the presence of a favourable pressure gradient. It is likely that the vorticity flux rate reaches the maximum value not at $X = 0$ but slightly downstream because the streamline curvature effect is significant for the separated shear layer in the region.

The above analysis illustrates that the mean vorticity flux rate can be obtained from the pressure distributions on the wall and in the free stream. In comparison with figure 7, figure 16 demonstrates an advantage of the present integral analysis in that it is capable of revealing streamwise variations of the mean vorticity flux rate without laborious velocity measurements in the flow field.

7. Conclusions

According to the data obtained for the vorticity flux rate, the oscillating plate enhances the time-mean vorticity flux rate in the region immediately downstream of the plate, but further downstream, i.e. $X/H > 10$, the time-mean vorticity flux rate returns to the reference value of the boundary layer without an oscillating plate. On the other hand, the data show that large variations of the ensemble-averaged vorticity flux rate are sensed when the vortices pass through the streamwise measurement location, even in the region $X/H = 10$ to 30. Hence, the oscillating plate plays the role of regulating the vorticity flux rate with respect to time.

A definition of vorticity distribution factor is proposed in this study, which is found useful for describing the effect of the oscillating plate displacing the vorticity away from the wall. It is found that this displacement effect is significant compared to the case without the oscillating plate. The ensemble-averaged results of this quantity further suggest that the vortical structure produced by the oscillating plate reaches a mature stage in the region $X/H = 10$–30.

The results obtained by the split-fibre probe near the wall show that multiple zero-velocity points can be identified in the cases with the oscillating plate. These points can be classified into reattachment (impingement) points and separation point. The characteristic size of the vortical structure can be estimated from the streamwise distance between the first and second zero-velocity points. The higher the K value, the more organized is the vortex produced by the oscillating plate and the shorter the measured streamwise distance between the first and the second zero-velocity points. The convection speed of the reattachment point is not constant through the oscillating period. In the initial stage of the upstroke motion of the oscillating plate, the convection speed is low, which corresponds to the stage of vorticity accumulation in the primary vortex. Later, but still in the upstroke motion, the convection speed increases, which corresponds to a stage when the separated shear layer contains multiple vortices. When the plate is in the downstroke motion, the convection speed further increases.

The effects of K on the measured wall pressure distribution can be summarized in two points: the higher the K value the lower the minimum wall pressure measured; and the higher the K value the closer the location of the minimum wall pressure is to the oscillating plate. This trend agrees with the flow visualization results that the higher the K value the more organized and smaller scale is the vortical structure developed behind the oscillating plate.

An integral analysis of the momentum equation indicates that the mean vorticity flux rate comprises contributions from both the parallel shear layer and the curving streamline. This analysis further suggests that a combination of the pressure measurements in the irrotational region of flow and on the wall can conveniently predict the mean vorticity flux rate upstream and downstream of the oscillating plate.

This work was supported by the National Science Council, Taiwan, Republic of China under grant number NSC 83-0401-E006-008.

REFERENCES

CHEN, C. R. 1991 Effects of a two-dimensional oscillating fence on boundary-layer development. MS thesis, Institute of Aeronautics and Astronautics, National Chen Kung University, Tainan, Taiwan.

DOLIGALSKI, T. L. & WALKER, J. D. A. 1984 The boundary layer induced by a convected two-dimensional vortex. *J. Fluid Mech.* **139**, 1–28.

EATON, J. K. & JOHNSTON, J. P. 1982 Low frequency unsteadiness of a reattaching turbulent shear layer. In *Turbulent Shear Flows 3* (ed. L. J. S. Bradbury, F. Durst, B. E. Launder, F. W. Schmidt & J. H. Whitelaw), pp. 162–170. Springer.

FRANCIS, M. S., KEESEE, J. E., LANG, J. D., SPARKS, G. W. & SISSON, G. E. 1979 Aerodynamic characteristics of an unsteady separation flow. *AIAA J.* **17**, 1332–1339.

KIYA, M. & SASAKI, K. 1983 Structure of a turbulent separation bubble. *J. Fluid Mech.* **137**, 83–113.

KIYA, M. & SASAKI, K. 1985 Structure of large-scale vortices and unsteady reverse flow in the reattaching zone of a turbulent separation bubble. *J. Fluid Mech.* **154**, 463–491.

KOGA, D. J. 1983 Control of separated flow fields using forced unsteadiness. PhD thesis, Illinois Inst. of Technology.

MIAU, J. J. & CHEN, M. H. 1991 Flow structures behind a vertically oscillating fence immersed in a flat-plate turbulent boundary layer. *Exps. Fluids* **11**, 118–124.

MIAU, J. J., CHEN, M. H. & CHOU, J. H. 1991*a* Frequency effect of an oscillating plate immersed in a turbulent boundary layer. *AIAA J.* **29**, 1068–1074.

MIAU, J. J., LEE, K. C., CHEN, M. H. & CHOU, J. H. 1991*b* Control of separated flow by a two-dimensional oscillating fence. *AIAA J.* **29**, 1140–1148.

NAGIB, H. M., REISENTHEL, P. H. & KOGA, D. J. 1985 On the dynamical scaling of forced unsteady separated flows. *AIAA Paper* 85-0553.

REISENTHEL, P. H., NAGIB, H. M. & KOGA, D. J. 1985 Control of separated flows using forced unsteadiness. *AIAA Paper* 85-0556.

REYNOLDS, W. C. & CARR, L. W. 1985 Review of unsteady, driven, separated flows. *AIAA Paper* 85-0527.

SEARS, W. R. 1956 Some recent developments in airfoil theory. *J. Aero. Sci.* **23**, 490–499.